

## Experimental and Analytical Investigation of Sand Production in Weak formations for Multiple Well Shut-Ins



Ashirgul Kozhagulova<sup>a,\*</sup>, Nguyen Hop Minh<sup>b</sup>, Yong Zhao<sup>a</sup>, Sai Cheong Fok<sup>a</sup>

<sup>a</sup> School of Engineering and Digital Sciences, Nazarbayev University, 53 Kabanbay batyr avenue, Astana, Kazakhstan

<sup>b</sup> Fulbright University Vietnam, 105 Ton Dat Tien, Ho Chi Minh City, Viet Nam

### ARTICLE INFO

#### Keywords:

Weak formation  
Sand production  
Experimental testing  
Analytical prediction  
Well shut-in  
Ustyurt-Buzachi

### ABSTRACT

Sand production is a severe problem in oilfields and is majorly associated with weak and unconsolidated formations. Therefore, identifying the expected amount and rate of sand has been approached by different analytical and numerical prediction methods. Within them the former requires less computational time and therefore being widely used. However, despite some of the analytical models proved to be fairly predictive for sand production during steady-state flow, they cannot be used directly for the wells with complex production profiles. The current study focuses on the experimental investigation of the sand production pattern during well production and shut-in periods. The laboratory work was conducted on artificial sandstone replicating weak Cretaceous formations in Kazakhstan using customized High Pressure Consolidation System (HPCS) for sand production experiments. HPCS accommodates a sandstone sample of a large diameter to diminish boundary effect when the fluid is injected. The tests were conducted at different overburden stresses as well as pressure drawdowns in several well shut-in runs. The paper presents a modification of the classical steady-state flow analytical solution incorporating field and fluid conditions as well as the dependence on the well shut-in runs. The model showed good convergence with the experimental and well data.

### 1. Introduction

Petroleum production from shallow clastic formations is often associated with wellbore instability and sand production. These undesirable effects not only cause damages to downhole equipment and surface treatment lines but also increase the operational cost due to more frequent well downtime. Therefore, comprehensive predictions are required to establish adequate sand production management and future contingency planning. Many of these models require calibration with data from small scale experiments. The studied shallow formations are both weak and porous. Sand production mechanisms have been widely studied in the past few decades and many theoretical and numerical models had been introduced to explain the phenomena based on simplified geometries and idealized assumptions. Regardless of the models, experimental results and field data analysis showed that sand production is mainly triggered by the well drawdowns and applied stresses changes (Araujo et al., 2014; Palmer et al., 2003; Papamichos et al., 2010, 2001, 2000; Papamichos and Malmanger, 2001; Willson et al., 2002).

The two main parameters associated with sand production prediction are 1) sanding onset and 2) sand production rate. Sanding onset can be estimated by studying stresses around wellbore (Bratli et al., 1983; Hayavi and Abdideh, 2017; Morita et al., 1989; Risnes et al., 1982; Yi, 2003; Zhang et al., 2016) and applying elasticity and plasticity theory. The borehole remains stable until a failure criterion is fulfilled by stresses around the wellbore. Depending on the material characteristics, shear failure criteria can be Mohr-Coulomb, Mogi-Coulomb, Tresca, Hoek-Brown, etc. (Colmenares and Zoback, 2002; Gholami et al., 2016; Rahimi and Nygaard, 2015). The applicability of the chosen failure criteria to a particular rock can be estimated from the failure envelope based on the triaxial shearing tests (Colmenares and Zoback, 2002). Beyond sanding initiation, an expected sand production rate also has to be derived. Pure erosion models (Papamichos and Malmanger, 2001; Skjaerstein et al., 1997; Vardoulakis et al., 1996) or coupling of it with the elasticity and plasticity theories (Papamichos and Stavropoulou, 1998; Stavropoulou et al., 1998), can predict the erosion rate of the disaggregated sand particles. Coupled fluid flow with the plastic flow of granular matter offered alternative approaches (Geilikman et al., 1994;

\* Corresponding author.

E-mail addresses: [ashirgul.kozhagulova@nu.edu.kz](mailto:ashirgul.kozhagulova@nu.edu.kz) (A. Kozhagulova), [hopminh.nguyen@fulbright.edu.vn](mailto:hopminh.nguyen@fulbright.edu.vn) (N.H. Minh), [yong.zhao@nu.edu.kz](mailto:yong.zhao@nu.edu.kz) (Y. Zhao), [scfokky@yahoo.com.au](mailto:scfokky@yahoo.com.au) (S.C. Fok).

van den Hoek and Geilikman, 2005, 2003).

The limitation of the analytical models is that they solve the equilibrium equation for discrete points in time. There is an inherent assumption that applying some stresses to the system will lead to a certain failure and only higher stresses can lead to change in the system. Sand production models are based on the assumption that the rock around the well follows a simple stress-path, i.e. increase in drawdown and flowrate or reservoir depletion. In practice, oil wells follow complex stress-paths during their lifetime with changes in reservoir pressure conditions, and the principal stresses redistribution around the wellbore. One example is the multiple well shut-ins that are executed during well workovers whereby sand can be produced. In the works by (Al-Awad (2001); Morita et al., 2006, 1989) the authors showed that there is an additional sand production with every new repetitive well shut-in. However, the response of the near-wellbore rock due to multiple well shut-ins and the effect on the sand production has not been well studied, apart from the field observations and simple laboratory work. This paper presents an experimental study of sand production triggered by pressure fluctuation in order to understand how repeated well shut-in runs affect sand production. The work focused on the weak Cretaceous sandstones. The tests were performed on artificial sandstones similar to weak Cretaceous reservoir sandstone in terms of strength and porosity-permeability parameters. The sand production experiments were conducted using a specially designed High Pressure Consolidation System (HPCS). The specimen is prepared in-situ and several tests conducted at different vertical stress levels and fluid flow rate. The fluid is injected from the periphery to the central hole of the specimen and liquid-sand mixture is captured at the outlet and analyzed. Each test consisted of several runs of well flowing and shut-ins periods, which were kept for sufficient time for stabilization. The experimental tests results showed that both applied stress and fluid rate affects sand production, which confirms the conclusions of other research in the field (Papamichos et al., 2001; Wu et al., 2016; Younessi et al., 2013). The data obtained during experiments helped to improve the existing widely accepted model for sand rate prediction (Geilikman et al., 1994).

## 2. Overview of oil field and a well production profile

Sand production from Kazakhstani oil fields is associated with shallow poorly consolidated formations in the Ustyurt-Buzachi sedimentary basin, which is situated between the Caspian Sea and Aral lake (Fig. 1) (Iskaziyev et al., 2013). Stratigraphically the oil-prone sections consist of Middle Jurassic rocks deposited on the eroded lower Triassic layer and Lower Cretaceous deposits lying on the Jurassic unconformities surface. Cretaceous sandstones are prone to sanding. These sandstones are composed mainly of loose sand and weakly cemented sandstones. Biostratigraphy showed that the sandstones were deposited in a lagoon-continental environment (Murzagaliyev, 2009). The porosity-permeability properties of the reservoir rocks, therefore, are quite high which can be explained by the shallow depths of the oil-pay layers of about 300–400 m. Porosity is about 30–35% and permeability –around 200–500 mD.

Fig. 2 illustrates the production profile for a cased and perforated well situated in the Ustyurt-Buzachi for 24 years from 1992 to 2016 (from well reports). There were no sand screens installed in this well, which is not an uncommon approach in the investigated field. It can be seen that till 2002 the flow was not sufficient enough and there was no sand produced. The oil production rate increased in 2002 and kept relatively constant until 2007 when the well was shut down for a while. Prior to the shut in, sand production showed a decreasing trend with some occasional bursts. However, after the well was brought back to production, there was a new trend of sand outbursts despite the fact that the flow rate's magnitude did not exceed the rate before shut down. The trend of sand production from repeated well shut-ins after 2007 was different from its previous stage and the sand produced cannot be accounted for in the models established to date, since there is no progressive pressure drawdown increase. To understand the phenomenon, experimental work described in the following sections was conducted to simulate multiple well shut-ins to determine their effect on the total sand production prediction.

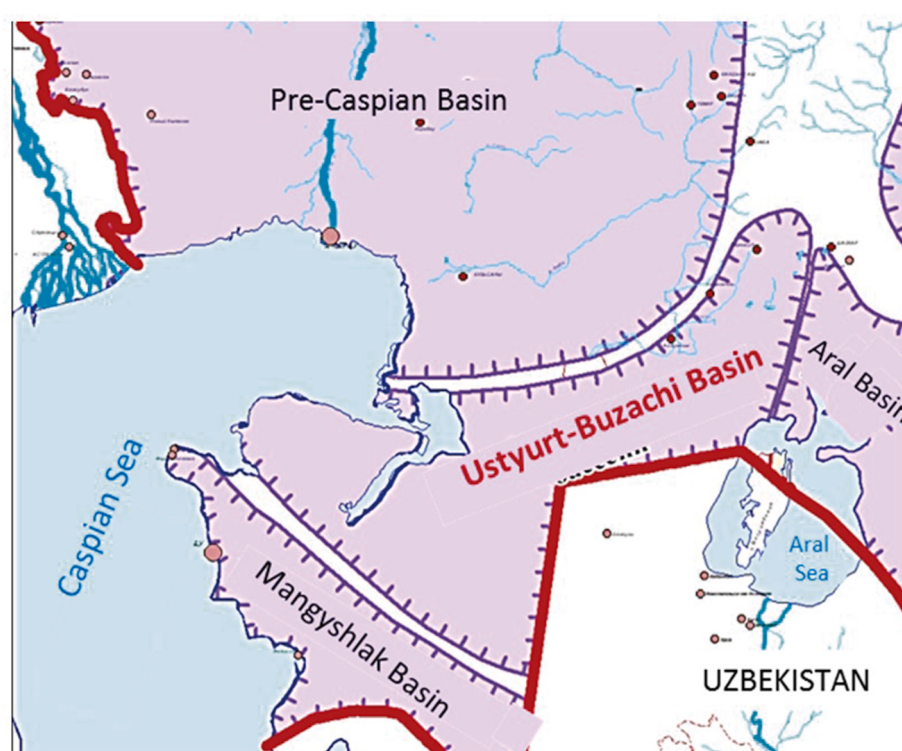
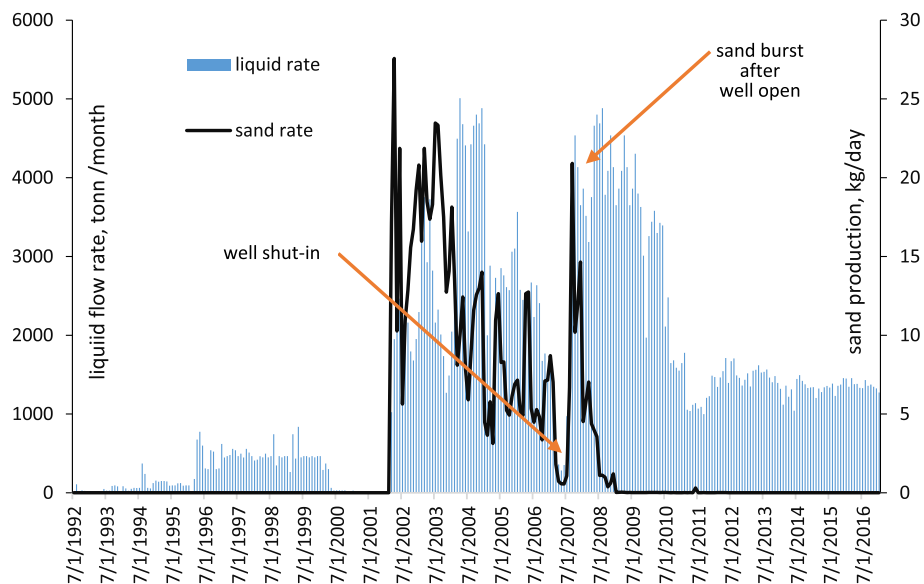


Fig. 1. The situation of Ustyurt-Buzachi sedimentary basin (after Iskaziyev et al., 2013).



**Fig. 2.** A typical Ustyurt-Buzachi oil well in production profile.

### 3. Experimental set-up- High Pressure Consolidation System

The large-scale laboratory sand production test was conducted using High Pressure Consolidation System (HPCS) (Fig. 3a and b). The HPCS is a large scale modified Rowe Cell system for wellbore instability testing (Kozhagulova et al., 2020b). It is equipped with the Servo-hydraulic Compression Load Frame, which allows compressing the specimen up to 5000 kN, followed by radial and axial fluid injection of up to 7 MPa

pressure at up to 5 l/min fluid flow rate. The HPCS is computer-controlled and consists of the following main parts: High Pressure Consolidation Cell, a pressurized fluid supply system, a produced fluid collection system, a solid separation system, and controlling software. The schematic and the general view of the apparatus is shown in Fig. 3a. The prepared specimen in the High Pressure Consolidation Cell is consolidated by applying stress in the vertical direction. The cell can accommodate a specimen of 300 mm in diameter and 240 mm in

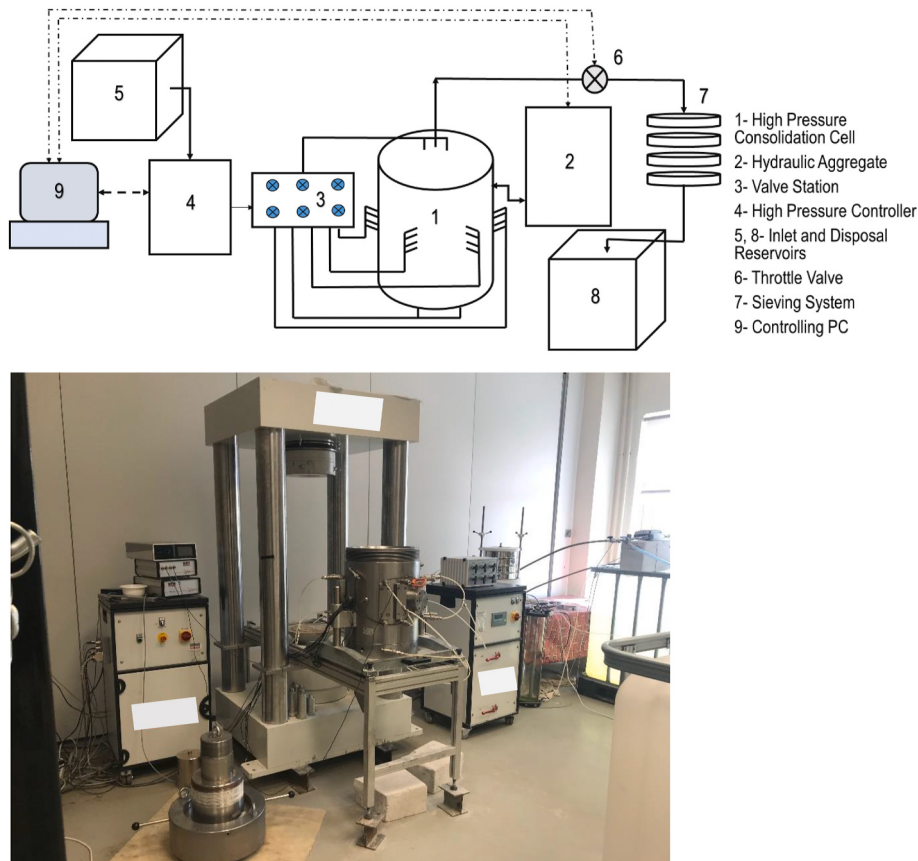


**Fig. 3.** a) Schematic and b) General View of High Pressure Consolidation System.

height.

In order to investigate the sanding onset as well as the volume of solids produced, the system allows the independent control of injected fluid pressure and the stress conditions. The injected fluid flows through the porous media of the specimen towards the center, from which it is transmitted to the fluid collection system. Two tanks, each of 1 m<sup>3</sup> in volume, supply the fluid for the radial and axial liquid injection.

For the experiment, the sample was prepared and cured in-situ. The specimen was then saturated with fluid. The saturation of the specimen is confirmed by the response of the pore water pressure change to the change in vertical stress. When the maximum pressure is reached, the safety valve is activated, which maintains injection pressure at the maximum possible level, with a precision of 0.5%.

The supplied liquid passes through the station valve, which allows activating/deactivating particular injection ports, therefore controlling the direction of fluid injection. The saturation stage was followed by the perforation, during which the specimen was penetrated to create a hole in its center. After the first cleanup, e.g. removal of the debris generated during perforation, the produced liquid-solid mixture was passed through the soil collection system.

The sand produced from the central hole fluid was then collected. The sieved sand particles were then collected and dried for future qualitative and quantitative analyses. The solid particles were analyzed in terms of amount, mass, shape, and the mineralogy of the grains.

During the experiment, the fluid flow rate can be either computer or manual controlled. In both cases, the flow rate is not dependent on the load control and any injection program can be implemented. The flow rate is controlled by the pressure drawdown, which is the difference between the inlet pressure and outlet pressures.

#### 4. Experimental procedure

##### 4.1. Testing materials

Cretaceous formations of Ustyurt-Buzachi sedimentary basin are highly porous and permeable which is conditioned by the shallow depth of the deposits and continental depositional environment. Petrophysical and fluid parameters for the Cretaceous sandstones are available in the field reports. The shallow wells are usually drilled many years ago, with no preservation of the intact core samples. The recent cores evacuated from the field usually lack integrity and therefore are not suitable for mechanical testing. For the experiment, artificial sandstones had to be produced.

For sample preparation quartz sand similar to the field sand particle distribution was chosen with the mean grain size D<sub>50</sub> = 0.3 mm and the solids specific gravity of around 2.65. The sand has the coefficient of uniformity equal to 2.0 and the coefficient of curvature equal to 0.89.

The sand was cemented with a sodium silicate solution. The sand and the solution were mixed and the mixture was placed in High Pressure Consolidation Cell. Circulating carbon dioxide through the unsolidified molded mixture resulted in the formation of silicate acid. This created the weak bonds between the individual grains. After solidification, the weakly bonded sandstone material was manufactured with a porosity of around 35% and permeability around 300mD similar to the studied reservoir rock. Mechanical testing and DEM results of this type of artificial sandstone was presented in the previous work of the authors (Kozhagulova et al., 2020a, 2018) and was found to have the main parameters summarized in Table 1.

##### 4.2. Specimen preparation, saturation and perforating the central opening

For large-scale sand production experiments, the specimen was prepared using 10:1 proportion of commercially available sand and sodium silicate cement as described in the preceding section.

The sand-cement mixture was then placed in the High Pressure Consolidation Cell (HPCC), which was preliminary internally covered

**Table 1**  
Main parameters of sandstone specimen.

Parameter	Value
Composite sand mean grain size, mm	0.3
Solids specific gravity	2.65
Coefficient of uniformity	2.0
Cement agent	Sodium silicate
Porosity, %	35
Permeability, mD	250–300
Friction angle, <sup>0</sup>	38.3
Cohesion intercept, kPa	250
Dimensions: height and diameter, mm	216 and 300
Hole radius, mm	7

with the filter paper for even distribution of the injected water and to prevent the cross-flow of the fine sand between the injection ports and the specimen outer boundary section. The mixture was placed in HPCC in several layers as widely practiced in the artificial specimen preparation (Consoli, 2014; Rios et al., 2014) and lightly compacted afterward. After the HPCC was placed under the HPCS frame, vertical load was applied until the compaction ratio achieved 1% of the initial mixture filling level. This ensured the absence of voids and gaps between the HPCS top cap and the surface of the specimen. After the consolidation had set for about 16–18 h, carbon dioxide gas was percolated via the injection ports from bottom and circumference at 5 bars for 20 min to solidify the cement and bond the particles together. The mechanism and the chemical reaction is explicitly described in (Kozhagulova et al., 2018). The porosity of the material in this study was calculated to be  $\varphi = 0.35$ . An unconfined compressive strength of a smaller size sample was tested to be 1.1 MPa, with shear strength S<sub>0</sub> of 0.25 MPa, which according to Fjaer et al. (2008) considered to be a very weak rock. After the preparation stage, the top cap was removed uncovering the surface of the specimen. A donut-shaped filter paper was secured onto the surface (Fig. 4c) to prevent undesirable disaggregation of particles from the surface.

In the next stage, the specimen was flushed with water injected from the bottom. The injection rate was set at 0.1–0.2 l/min and the percolation lasted for 20–24 h. The central opening was then created with a 14 mm diameter electric drill.

##### 4.3. Test procedure

After the sample was prepared, saturated with water and perforated, overburden stress of a certain magnitude was then applied to reconstitute field conditions at 5 kPa/s. The horizontal stresses increased as a response to the overburden stress and their value was measured by the transducers mounted to the rigid wall of the specimen cell. The maximum values for both overburden and horizontal stress values are summarized in Table 2. Sand debris was collected by injecting water from the bottom of the specimen. The flow rate was sufficient to lift the sand particles through the central hole. In order to understand the sand production behavior during unsteady flow conditions, the experiments were conducted in several well flow and well shut-ins alternating runs (Fig. 5).

Each run consisted of the two following stage after certain vertical stress is applied:

- (a) Well shut-in: Fluid injected under certain pressure with outlet valve closed allowing no outflow – 40 min;
- (b) Well flowing: A constant drawdown pressure is applied via opening outlet valve - 40 min;

During the shut-in stage fluid pressure builds up around wellbore and fluid pressure is assumed to equilibrate across the sample due to the small size of the sample in comparison with the field scale. During the well-flowing stage, the disaggregated sand particles were transported

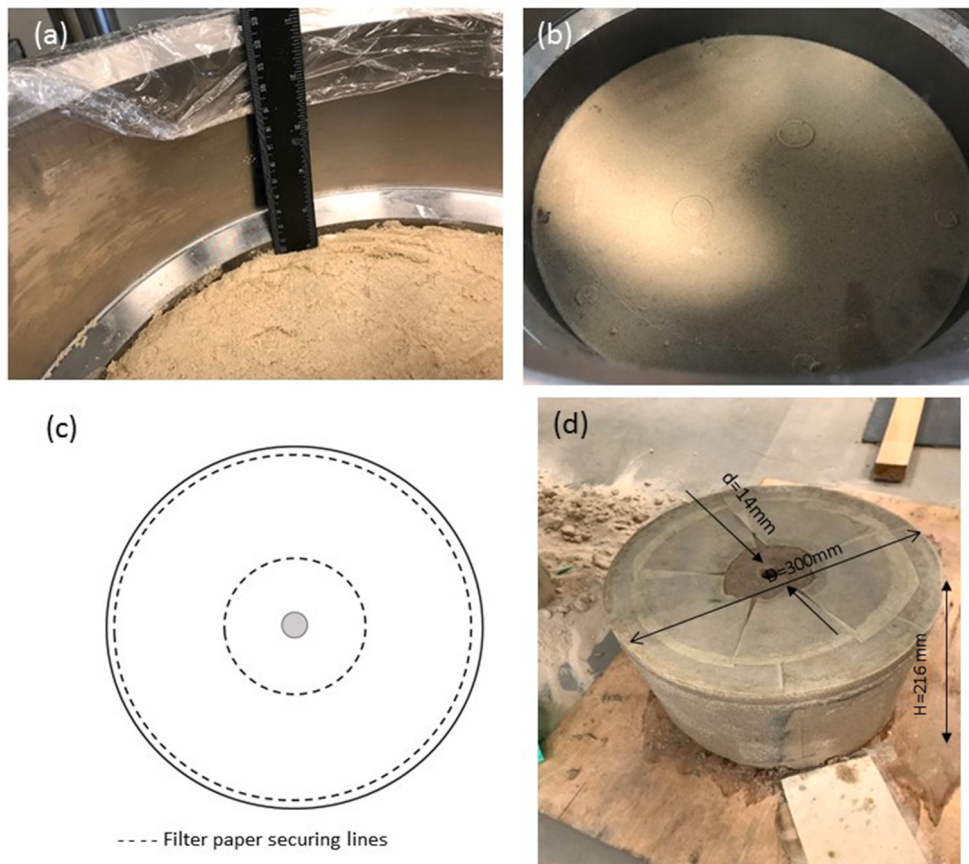


**Fig. 4.** Specimen preparation illustrations: a) Sand-cement mixture surface; b) Consolidated surface; c) Top view- filtre paper gluing lines; d)A typical specimen

**Table 2**  
Tests summary.

TEST	OVERBURDEN STRESS $\sigma_v$ , kPa	HORIZONTAL STRESS $\sigma_h$ , kPa	DRAWDOWN $\Delta p$ , kPa	FLOW RATE Q, L/MIN	NUMBER OF SHUT-IN RUNS
A	3000	1260	500	1.3	1
B	4000	1510	500	1.25	1
C	4000	1510	900	2.6	5
D	4000	1510	1300	3.2	5
E	5000	1960	1200	2.5	5
F	5000	1960	1850	4.0	7

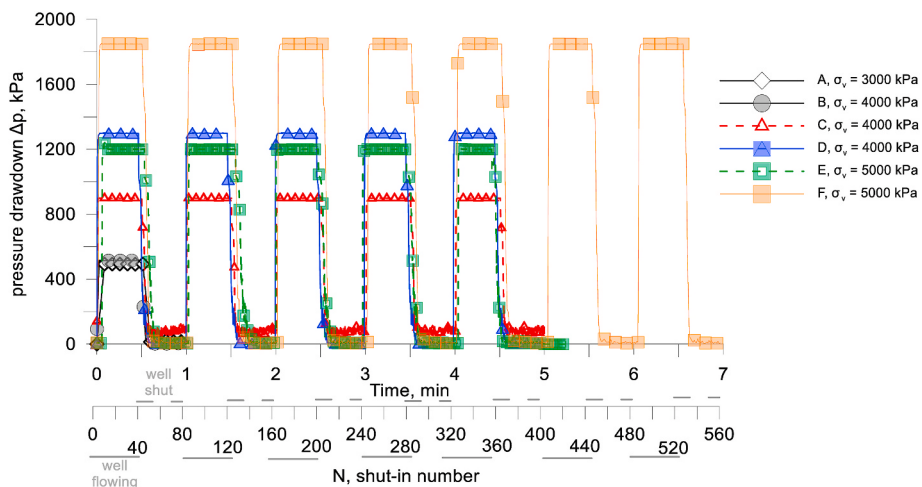


**Fig. 5.** Applied pressure drawdown paths.

via fluid flow and captured with a sieving system. Even though the major sand production is associated with the beginning of the flow and became less than 1 g/h after the first 20 min, the flow continued for 40 min in total for each run to ensure no additional sand production or any unexpected sand breakthrough. The sand was collected in several portions and then oven-dried for 24 h. After 40 min, the outflow valve was slowly closed to avoid any impulse effect. It was kept shut for 40 min in order to achieve pressure equilibration. After that outflow was continued by opening the outlet valve and establishing the pressure difference at the same level as in the previous run. Each test was conducted in 1–7 runs (Table 2).

**Table 2** summarizes the setups of tests in terms of applied total overburden and horizontal stresses, well drawdown pressures, and fluid rates.

## 5. Experimental results and discussion

Sand collected in time intervals during the experiment was oven-dried and weighted. The masses were summarized within each test to understand the magnitude of sand produced for each shut-in run. Figs. 6–10 display the sand production information on all the tests A–F as dependence on time and shut-in run number.

As can be seen from Fig. 6, tests A and B showed very little sand: less than 0.2 g, which can be considered to lie within the error range of the experiment. Tests C and D were conducted at 4 MPa vertical stress and the sand produced during the first shut-in run is greater than 50% of the total sand produced during each subsequent shut-in. For Test E conducted at 5 MPa vertical stress, the sand produced in the second to fifth shut-ins was still significant and did not decline to zero. For test F, which has been also conducted at 5 MPa vertical stress, but at larger drawdown pressure, the sand produced kept its magnitude at around 70% of the first shut-in runs magnitude. It can be concluded that the sanding magnitude depends both on the solid stress conditions as well as the fluid flow parameters.

Fig. 7 displays the cumulative sand production for each test, including an enlargement inset for tests A and B. No additional sand production was observed for these tests, therefore a conservative view on sand production prediction is fairly suitable. This implies that resuming and restarting the well will not cause additional sand to be produced. In its turn, sand production for tests C and D shows a gradual leveling, therefore one can conclude that the subsequent shut-in runs would produce more sand though in a diminishing manner. The results

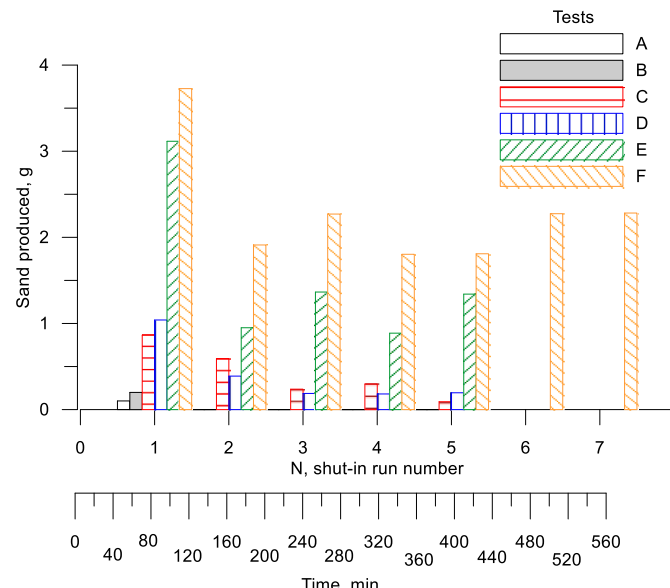


Fig. 6. Sand mass produced during every shut-in.

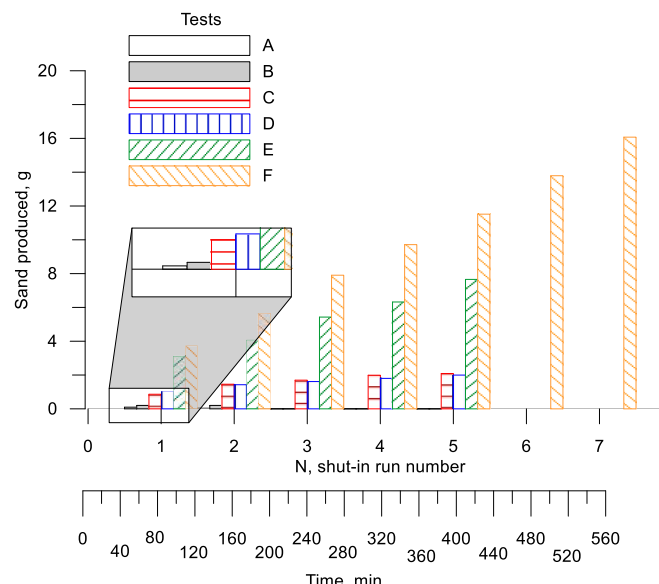


Fig. 7. Cumulative sand production.

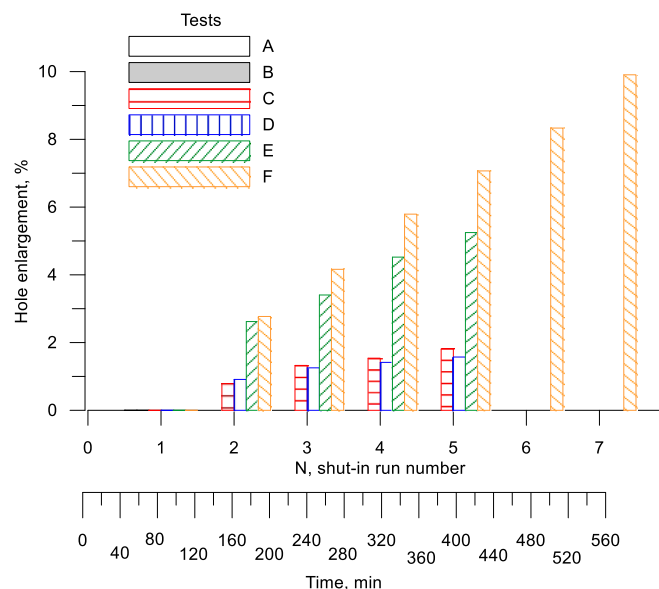


Fig. 8. Hole enlargement.

indicated that after vertical overburden stress had been exceeded, the magnitude of the vertical stress and the applied pressure drawdown will affect sand production. The observations for tests E and F also confirmed the previous indications, and each shut-in run resulted in additional substantial sand production increments. The increment magnitude is higher for test F compared with test E, therefore it is more important for higher pressure drawdowns rather than the lower values.

Fig. 8 represents the relative enlargement of the central hole in percentage after each subsequent shut-in run. HPCS is not equipped with the internal radial strain gauges to capture the enlargement of the hole directly and the enlargement of the hole was calculated based on the produced sand mass. For simplicity, an even detachment of sand grains from the wellbore surface was assumed. We can see that the similar to cumulative sand production value, the hole enlargement is not very significant for tests C and D, which is around 1.5%. The enlargement of the hole for tests E stabilized at around 5%. As expected, the maximum enlargement of the hole was observed for test F which increases at about 1.5% after each shut-in, resulted in 10% enlargement after 7 runs. As the

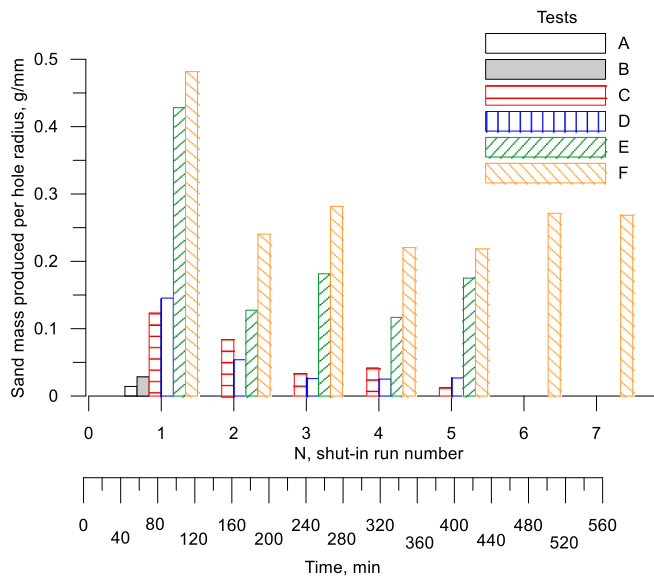


Fig. 9. Sand produced per hole radius, g/mm.

initial hole radius is known to be an important parameter for sand prediction, as an easy estimation for possible larger or smaller hole radii, Fig. 9 shows the sand mass produced per hole radius, which trend is consistent with the nominal sand production trend in Fig. 6.

Since the tests A and B did not show any significant sand production, only tests C–F results will be considered for prediction in the analysis. Fig. 10 shows the experimental data of the sand rates for tests C–F in terms of the well shut-in runs.

When the material around the hole is broken, the initial flow drags sand particles towards the hole, and gradually the particles start to clog the pore throats leading to the decreased permeability in the near-wellbore zone. However, the porosity and permeability increase as sand being produced. The well shut-in causes stress redistribution and particle rearrangement, which lead to a new portion of the detached particles be produced after the well is brought to production again. As it is known, from elasticity and plasticity theory, the plastic zone front

propagation depends on the far-field stress as well as the pressure drawdown. Equivalently, as it is seen from the experimental data, the level of the sand burst after the first shut-in run also depends on the combination of the field stress and the pressure drawdown: conducted at the same overburden stress tests E and F showed slightly different additional sand production data.

## 6. Prediction model

It is accepted that no sanding is expected from intact rock, even if it is poorly consolidated, because the fluid flow is not capable of disaggregating the sand grains from its matrix (Fjaer et al., 2008), unless the rock is damaged. However, after the well is drilled and brought to production, stresses start to transform around the hole, and rock around a wellbore starts to get plastified due to damage. This stress transformation depends on the magnitude of the applied effective stresses as well as the force of the fluid entering the wellbore. If the drag force is sufficient enough to carry disaggregated particles, sanding onset is expected. Fig. 11 illustrates the stresses distribution around the drilled hole. Based on the theory of elasticity and plasticity (Bratli et al., 1983; Fjaer et al., 2008; Risnes et al., 1982) and its combination with the appropriate failure criteria, one can estimate hole failure and sanding onset. When the failure criteria have been fulfilled a plastic zone appears around the wellbore and the radius of the plastic zone can be calculated. It should also be noted that in the presented experimental work, the minimum and maximum horizontal stresses are almost equal, therefore the standard calculation of stresses around the borehole is applicable. The cases when the horizontal stresses are not comparable with each other have not been tested by the given in this study approach.

To quantify if the material failure around hole has been achieved at the current stress state and pressure drawdown, the stresses in elastic and plastic zones can be calculated separately using Eqs. (1–3) and (4–5) respectively for every distinct radial point  $r$  between wellbore  $R_i$  and outer radius  $R_o$ .

Stresses in elastic zone:

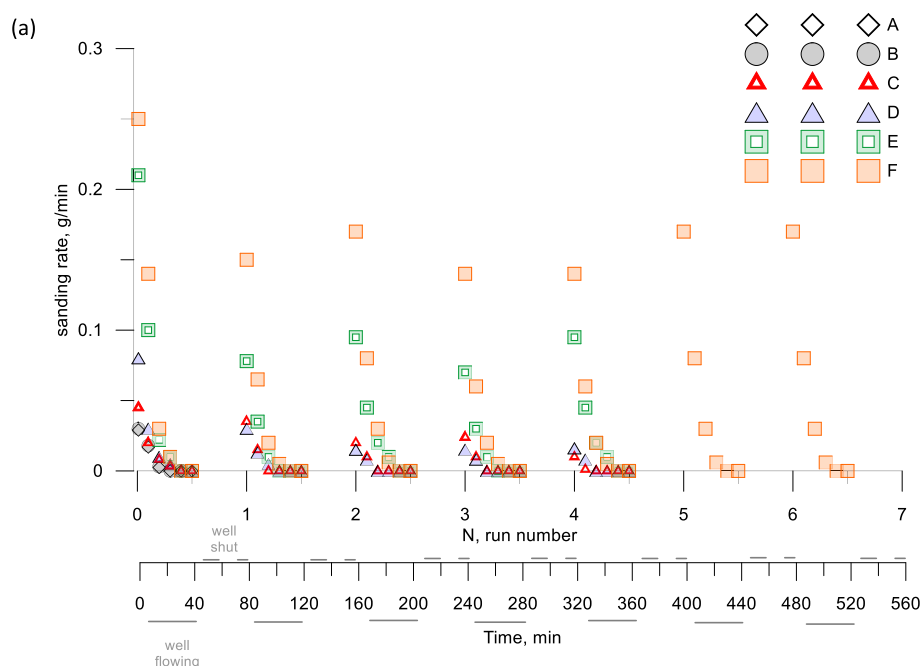
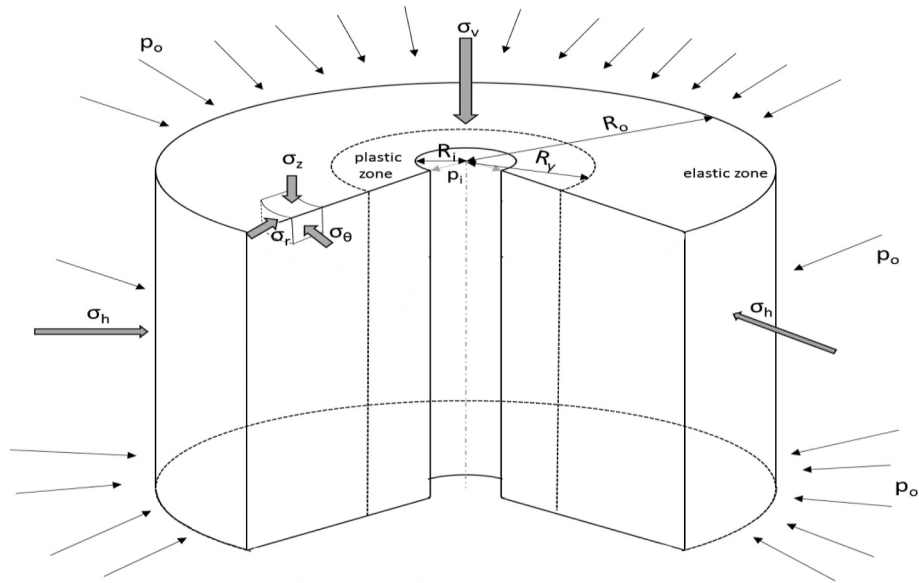


Fig. 10. Experimental data on sand production rate.



**Fig. 11.** Stresses around drilled hole illustration.

$$\sigma_r = \sigma_h + (\sigma_h - p_i) \frac{R_i^2}{R_o^2 - R_i^2} \left[ 1 - \frac{R_o^2}{r^2} \right] - (p_o - p_i) \eta \left\{ \frac{R_i^2}{R_o^2 - R_i^2} \left[ 1 - \frac{R_o^2}{r^2} \right] + \frac{\ln \frac{R_o}{r}}{\ln \frac{R_o}{R_i}} \right\} \quad (1)$$

$$\sigma_\theta = \sigma_h + (\sigma_h - p_i) \frac{R_i^2}{R_o^2 - R_i^2} \left[ 1 + \frac{R_o^2}{r^2} \right] - (p_o - p_i) \eta \left\{ \frac{R_i^2}{R_o^2 - R_i^2} \left[ 1 + \frac{R_o^2}{r^2} \right] + \frac{\ln \frac{R_o}{r} - 1}{\ln \frac{R_o}{R_i}} \right\} \quad (2)$$

$$\sigma_z = \sigma_v + 2\nu_{fr}(\sigma_h - p_i) \frac{R_i^2}{R_o^2 - R_i^2} - (p_o - p_i) \eta \left\{ \frac{2\nu_{fr}R_i^2}{R_o^2 - R_i^2} + \frac{2\ln \frac{R_o}{r} - \nu_{fr}}{\ln \frac{R_o}{R_i}} \right\} \quad (3)$$

, where  $\sigma_r$ ,  $\sigma_\theta$ ,  $\sigma_z$  are radial, tangential, axial stresses at radial distance  $r$  from hole;  $\sigma_h$ ,  $\sigma_v$  are far field horizontal and overburden stresses;  $R_i$ ,  $R_o$  are internal and outer radii of the specimen;  $p_i$ ,  $p_o$  are fluid pressures at inner and outer boundaries;  $\eta$  is the compressibility constant;  $\nu_{fr}$  is drained Poisson's ratio.

Stresses in the plastic zone:

$$\sigma_r = p_i + \frac{\mu q}{2\pi L k_p} \ln \left( \frac{r}{R_i} \right) + \frac{1}{tt} \left( 2S_0 \tan \alpha - \frac{\mu q}{2\pi L k_p} \right) \left[ \left( \frac{r}{R_i} \right)^tt - 1 \right] \quad (4)$$

$$\begin{aligned} \sigma_\theta = \sigma_z = p_i + \frac{\mu q}{2\pi L k_p} \left( 1 + \ln \left( \frac{r}{R_i} \right) \right) \\ + \frac{1}{tt} \left( 2S_0 \tan \alpha - \frac{\mu q}{2\pi L k_p} \right) \left[ (tt+1) \left( \frac{r}{R_i} \right)^tt - 1 \right] \end{aligned} \quad (5)$$

, where  $\mu$  is fluid viscosity,  $q$  is the fluid rate,  $L$  is drainage height,  $k_p$  rock permeability in the plastic zone,  $r$  is the radial distance from hole to the outer boundary;  $S_0$  is inherent shear strength;  $tt = \tan^2 \alpha - 1$ ,  $\alpha$  – failure angle

After the stresses are calculated for every radial point  $r$ , the plastic zone is assumed to exist as long as the failure criterion is satisfied. For simplicity, we used the Mohr-Coulomb failure criteria (Eq. (6)) for the material used in the experimental part.

Mohr-Coulomb failure criteria:

$$\sigma'_1 = 2S_0 \tan \alpha + \sigma'_3 \tan^2 \alpha \quad (6)$$

, where  $\sigma'_1$  is the major principle effective stress in the elastic zone and  $\sigma'_3$  is the minor principle of effective stress in the plastic zone.

Solving Eq. (6) for  $r$  gives the value of plastic zone radius – the radial distance between the hole center and the boundary between the elastic and plastic regions and is further denoted as  $R_p$ . It is assumed, that sand is produced from the plastified zone only and cannot exceed its volume, but not obligatory to be evacuated totally.

For sand production prediction, it is important not only to know the extent of the plastic region in the cemented sand but also to anticipate the rate of sand produced. The prediction of sand production rate as a viscoplastic granular flow was presented in (Geilikman et al. (1994)) with further improvement by van den Hoek and Geilikman (2005, 2003). During the well start-up, the reduction of the well fluid pressure leads to the increase in the deviatoric stress near the wellbore region. If the applicable failure criterion is not satisfied, the well conserves its stability. Changes in the applied stresses or fluid pressures can lead to the fulfillment of the failure criteria and subsequent yielding of the material near the wellbore. If the drag force of the fluid is sufficient, then sand flux is transported with the produced fluid towards the lower pressure region.

In the paper on the subject of viscogranular flow (Geilikman et al., 1994) the rate of produced sand was derived by the combination of the continuity equations with the radial Darcy's flow equation in porous media.

The main derivation steps will be recalled here based on the steady-state flow, but with the denotation of time dependence for the unsteady flow parameters for simplicity. The flow equation based on the combination of the amended Darcy's equation with the continuity equations will result in separate flow velocities for fluid and solids phases (Eq. (7)).

$$\frac{\partial p}{\partial r} = -\frac{\mu}{k} (v_f - v_s) \quad (7)$$

, where  $p$  is fluid pressure,  $r$  is the radial distance from hole center,  $\mu$  is fluid viscosity,  $k$  is porous media permeability,  $v_f$  is the fluid velocity,  $v_s$  is sand flux velocity.

Because fluid pressure and fluid flux are equal Eqn. (8) and (9):

$$\varphi v = \varphi_p k_p |_{r=R_p} \quad (8)$$

$$p_p(R_p) = p(R_p) \quad (9)$$

, where  $\varphi_p, \varphi$  are porosity values in plastic and elastic zones;  $p_p, p$  are fluid pressures in plastic and elastic zones.

Using the continuity equations, fluid velocity values for plastic (Eq. (10)) and elastic (Eq. (11)) zones can be approximated as following:

$$v_p(t) = -\frac{Q_p}{r} - \frac{1 - \varphi_p}{\varphi_p} v_s \quad (10)$$

$$v_f(t) = -\frac{Q(t)}{r} \quad (11)$$

, where  $Q_p, Q$  are volumetric flow rates in plastic and elastic zones;  $v_p(t), v_f(t)$  are fluid velocities in plastic and elastic zones.

Integrating Darcy's fluid flow equations separately for the yielded and non-yielded zones will give the respective volumetric rates  $Q_p$  and  $Q$ .

Because fluid flux and pressures are equal for plastic and elastic zones, fluid rates can be expressed through the solid rate  $q_s$  as a function of time:

$$Q(t) = \frac{\varphi_p}{\varphi} Q_p(t) - \frac{1 - \varphi_p}{\varphi} q_s(t) \quad (12)$$

And Darcy's equation for radial flow in plastic and elastic regions will take a form of the following:

$$p_p(r) = p_w + \frac{\mu}{2\pi L k_p} \left( Q_p(t) - \frac{q_s(t)}{\varphi_p} \right) \ln \frac{r}{r_w}, \text{ for } r \leq R_i; \quad (13)$$

$$p(r) = p_e - \frac{\mu Q(t)}{2\pi L k} \ln \frac{R_0}{r}, \text{ for } R_i < r < R_o \quad (14)$$

, where  $\varphi_p, k_p$  are minimum porosity and permeability in the plastic zone;  $\varphi, k$  are porosity and permeability at the elastic/plastic zone boundary;  $L$  is the drainage height.

Substituting flow rates for plastic (Eq. (13)) and elastic (Eq. (14)) to the total fluid flow rate equation (Eq. (12)) with the fluid velocity equations (Eq. (10)), (Eq. (11)) will give the equation for flow in the plastic zone in terms of sand rate. By rearranging it, sand rate  $q_s(t)$  can be expressed in terms of fluid flow rate in the plastic zone as following based on the propagation of the  $r$  plastic zone radius with time  $R_p(t)$  Eqn. (16) and (17):

$$q_s(t) = (Q_p(t) \times C - \Delta p) / D \quad (15)$$

, where the coefficients are:

$$C = \frac{\mu}{2\pi L} \left( \frac{1}{k_p} \ln \frac{R_p(t)}{R_i} + \frac{\varphi}{\varphi_p k_p} \ln \frac{R_0}{R_p(t)} \right) \quad (16)$$

$$D = \frac{\mu}{2\pi L} \left( \frac{1}{k_p \varphi_p} \ln \frac{R_p(t)}{R_i} + \frac{1 - \varphi}{k_p \varphi_p} \ln \frac{R_0}{R_p(t)} \right) \quad (17)$$

As it was stated earlier, the flow during the repetition of the well flow and shut-in alternating runs cannot be treated as steady-state flow. The flow pattern during well shut-ins and restarts is rather a repetitive chain of the ongoing flow and no flow sections, with the flow being stable within one section. Therefore, the fluctuation pattern of the flow may not have a simple solution, which means the analytical modeling might lose its main advantage - simplicity and prompt applicability. Nevertheless, the repetition characteristics of the flowrate curve can be approximated using Fourier series as a wave function with the following Eqn. (18), (19) and (20):

$$Q_p(t) = Q_p \times f(t) \quad (18)$$

$$f(t) = \begin{cases} 1, & (N-1)T < t < \left(N - \frac{1}{2}\right)T \\ 0, & \left(N - \frac{1}{2}\right)T < t < NT \end{cases} \quad (19)$$

$$\left\{ \begin{array}{l} f(t) \approx \sum_{j=0}^{\infty} a_j \cos\left(j \frac{2\pi t}{T}\right) + b_j \sin\left(j \frac{2\pi t}{T}\right) \\ a_j = f(t), \cos\left(j \frac{2\pi t}{T}\right) \\ b_j = f(t), \sin\left(j \frac{2\pi t}{T}\right) \end{array} \right. \quad (20)$$

where  $N$  is the number of shut-in runs,  $T$  is the period of each run,  $t$  is a timestep.

Fluid flow during multiple well shut-ins approximated by Fourier series for test C as an example is displayed in Fig. 12. It should however be noted that the noise around the discontinuities is usually about 7–8%.

For the initial well flow run, the permeability of the plastified zone  $k_p$  can be identified by knowing the initial permeability value  $k$  of the material and the average permeability  $k_{avg}$  based on the fluid rate from experimental or fluid data Eqn. (21).

$$\frac{\ln \frac{R_p}{R_i}}{k_p} + \frac{\ln \frac{R_0}{R_p}}{k} = \frac{\ln \frac{R_0}{R_i}}{k_{avg}} \quad (21)$$

In its turn, the porosity of the plastic zone can be evaluated based on Kozeny-Carman equation. Once the plastic zone is formed around the hole and the drag force is sufficient to carry the flux, the permeability profile follows a convex path as the flow stabilization progresses. Both porosity and permeability start to decrease due to the plastification of the material and then start to grow due to flux evacuation from the material skeleton. A more detailed theoretical explanation of the change in the porosity and permeability and their governing equations for the steady state flow, can be found in the paper by Shabdirova et al. (2020).

Even though the new well shut-in runs cause new sand to be produced, the stresses around hole do not exceed the maximum value of the previous run, because the main parameters in Eqs (2)–(6) are kept unchanged, therefore the plastic zone does not enlarge significantly with the number of well shut-in runs. However, rather a bigger proportion of sand is produced from the plastified zone.

Importantly, the propagation of the plastic zone front  $R_p(t)$  can be identified as the function of the plastic zone enlargement with the applied drawdown. Even though the drawdown is applied instantly, the flow rate takes some time for stabilization for finite geometry. During the experiments within the current study, the flow stabilization was established in about 7–10 min. With this time dependence of  $R_p$  can be established. The flow dependence with time would be governed by different equations depending on the material diffusivity. In the current study the following flow equation was obtained based on the

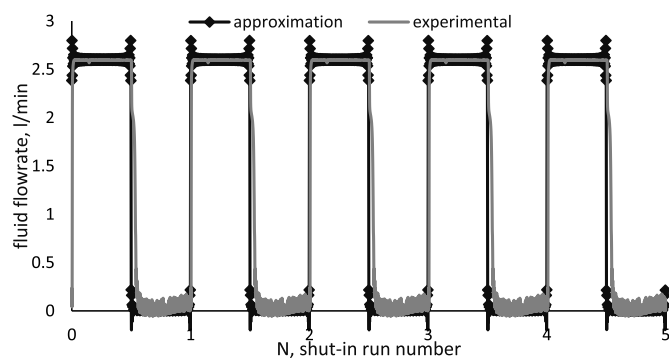


Fig. 12. Fourier transformation for fluid flow approximation during test C.

experimental findings Eqn. (22):

$$q_f(t) = q_f \times \left(1 - \frac{1}{2^{t/16}}\right) \quad (22)$$

In order to quantify the damping rate of the sand production trend, we will introduce the A coefficient of the sand bursts for well shut-in runs are incorporated to the (Eq. (15)) so as to capture the sanding rate shape as follows:

$$q_s(t) = A(Q_p(t) \times C - \Delta p)/D \quad (23)$$

Based on the experiments conducted, we can conclude that the damping pattern of the sand flow with the number of shut-in runs is straightly proportional to the level of the fluid drawdown and applied far-field stress combination. The damping rate also depends on the strength of the material, with the less sand to be detached for the stronger material. The number of well shut-in runs also plays an important role in the model and present the sand flow rate with every well shut-in, so the sand production damping rate is as follows, based on the experimental observations:

$$A = \frac{0.00003}{R_p(t)/R_p} \exp \left[ -N^3 \left( \frac{S_0}{S + \Delta p} \right)^2 \right] \quad (24)$$

where  $R_p(t)$  is the plastic zone propagation,  $S$  is the mean total far-field stress,  $N$  is the number of well shut-in.

Mean total far-field stress  $S$  in Eq. (23) is governed by the depth of the well (overburden stress) and horizontal stresses acting from far-field and can be calculated as follows Eqn. (25):

$$S = (\sigma_v + 2\sigma_h)/3 \quad (25)$$

Overall, the adopted for well shut-in model (Eq. (23)) takes into account the combination of the far-field stress with the applied pressure drawdown, in order to predict the diminishing or constant level of the additional sand to be produced.

Applying sand production rate equation (Eqs. (15), (18) and (23))

together with the sand damping rate coefficient (Eq. (24)) results in the prediction algorithm displayed in Fig. 13.

Following the displayed in Fig. 13 algorithm, one can predict the experimental data presented in Fig. 10. As it can be seen (Fig. 14), the model shows a good convergence with the experimental data in terms of peak and for the flow rate stabilization period, which brings more than 80% of the total sand produced for every well startup. Though it overestimates the constant sand rate after the flow stabilization and does not show the residual sand rate to approach 0 g/min.

As was stated before, the wells drilled deeper, therefore at a higher total far-field stress experience not diminishing but constant sand production pattern with every well shut-in. It should be noted that this effect is more pronounced as the well is shut-in for several times, e.g. N number of well shut-in runs is larger than 2.

To understand if the model can predict the sand rate not only in a laboratory scale but also in field scale, the following well data from Ustyurt-Buzachi (Fig. 2) will be analyzed.

### 6.1. Well data validation

To validate the model, the sand production from the well drilled in the Cretaceous formation of Ustyurt-Buzachi was chosen (introduced in Fig. 2). For an easier display, only the well production profile with a sufficient flow rate is selected from the beginning of the year 2002 till the end of the year 2010 (Fig. 15). Sanding profile of the well showed a typical trend of diminishing with time rate. Moreover, well flowing was stopped between the 60th and the 64th months. The well was brought to production at a similar before shut-in flow rate afterward.

The pay zone of the well is located between 292m and 313m true vertical depth resulted in 21m pay thickness. Giving the standard perforation shot density of 16 shots per each meter with 90° phasing, there are 336 perforations in the pay zone, with the following dimensions according to the perforation passport: diameter of 0.0166 m ( $R_i = 0.083$  m) and length ( $L$ ) of 2 m. The vertical distance between each two horizontal perforations is 0.25 m, therefore drainage radius ( $R_o$ ) was

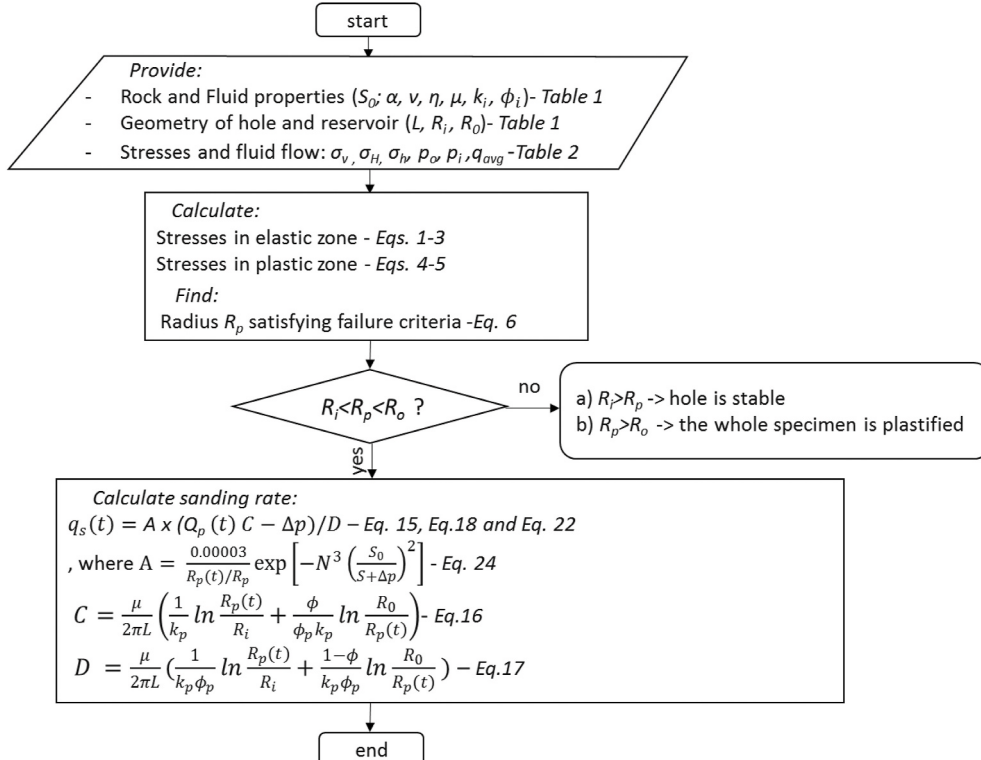
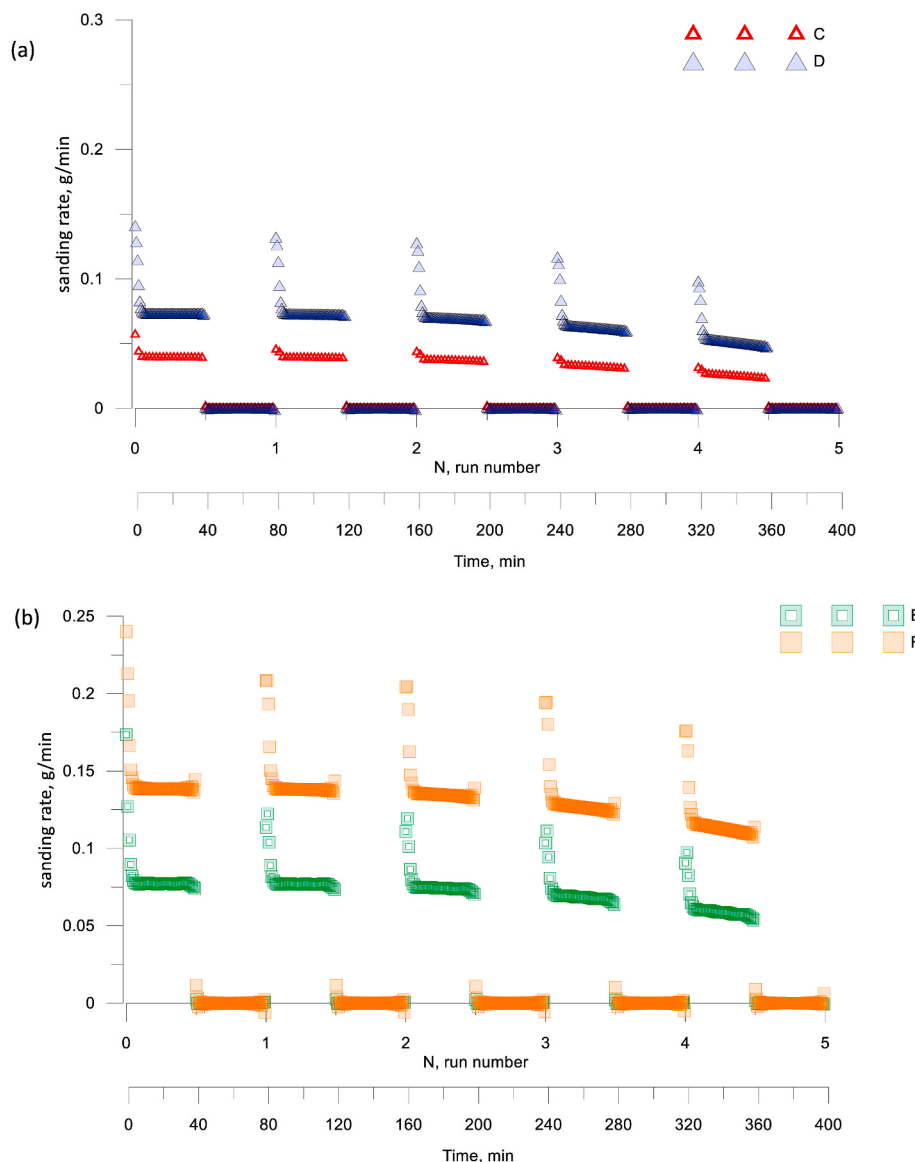
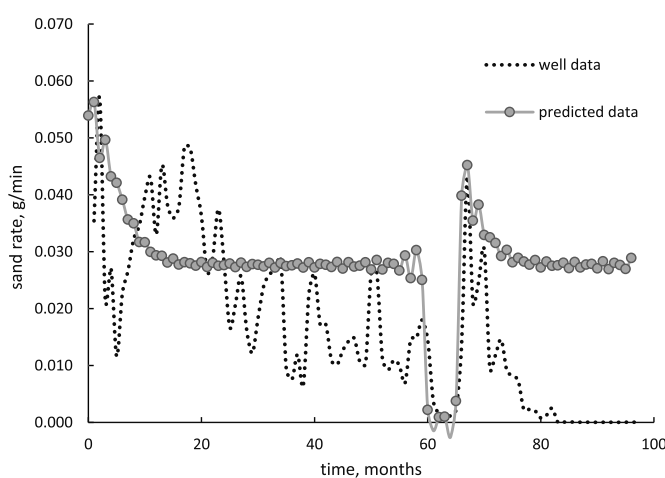


Fig. 13. Prediction algorithm.



**Fig. 14.** Predicted data on sand production rates for tests a) tests C, D and b) tests E, F.



**Fig. 15.** Actual and predicted sand flow rate per each perforation.

accepted to be half of this distance- 0.125 m. The pressure drawdown fluctuation is negligible for the given period; therefore the following mean values were accepted for the calculation: the outer boundary fluid pressure  $p_0$  is 2.2 MPa and the bottomhole flowing pressure  $p_i = 0.9$  MPa.

The prediction model presented in the previous section was developed for a vertically oriented hole, therefore stresses transformation calculation from a vertical to a horizontal hole Fig. A1 were performed (Appendix A Eqn. (A1), (A2) and (A3)), with inclination angle being equal to  $90^0$ .

Following the presented in Fig. 13 flowchart with the stresses transformation given in Appendix 1, the sanding rate of the well was predicted and compared to the actual sanding data (Fig. 15). Which was limited to the initial constant production period of 60 months with a short shut-in and restart at a similar flow rate.

As can be seen, the initial sand burst is predicted with fairly good precision, the downward trend is also similar to the well data. However, after the well stabilization, the model overpredicts the sand rate for about 50%. Moreover, the well sand production rate does not approach zero, as the model predicted data does. Nevertheless, the sand burst as the dependence on the applied drawdown and the total stress is

predicted with high precision. It allows anticipating the level of sand burst after a well shut-in for different purposes. However, as for the experimental data the model overpredicts the sand rate after the flow stabilization.

Analyzing application to the well scale, one can conclude that the presented analytical model proved to give a good estimation of the level of the sand burst for both initial production start and the production restart after well shut-in.

## 7. Conclusion

The paper presents a combined experimental and theoretical study on weak sandstone analog material of shallow formations. The experiments were conducted to repeat well shut-in and restart runs in a controlled manner. During experiments, it was observed that well shut-ins have a different level of influence on additional sand production depending on the operation conditions. The results showed that the additional sand production is more pronounced in the experiments operating under higher overburden stresses. There was also a positive correlation between the applied pressure drawdown level and sanding magnitude during well shut-in. An existing sanding rate prediction model applicable for steady-state flow was adopted and modified in the current study to predict the flow patterns and sanding rates for multiple well shut-ins using the Fourier series expansion of a square wave. The adaptation presented in this work takes into account the combination of the formation strength, applied solid stresses, and the fluid production pressures as being more or less influential for an order of well shut-in. A well data from Ustyurt-Buzachi sedimentary basin used for field-scale

applicability is also presented.

It was found that the newly modified model can reasonably produce the magnitudes of sanding rates for the initial production and after the well is brought to production after some time of not operating for both experimental and well data. However, the model showed a less accurate continuous sanding rate prediction in comparison with experimental data rather than well data, which might be associated with the limited geometrical boundaries. Nevertheless, it is found to be computationally efficient and easy to be applied for fast sanding rate estimation.

## CRediT authorship contribution statement

**Ashirgul Kozhagulova:** Data curation, Methodology, Formal analysis, Writing - original draft, Writing - review & editing. **Nguyen Hop Minh:** Conceptualization, Supervision. **Yong Zhao:** Supervision, Writing - review & editing. **Sai Cheong Fok:** Writing - review & editing.

## Declaration of Competing interest

The authors declare that they have no known competing financial interests or personal relationships that could have appeared to influence the work reported in this paper.

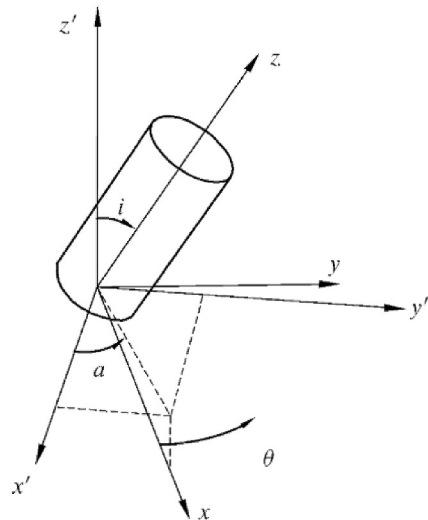
## 8. Acknowledgments

The project was supported by Nazarbayev University (research grant SOE2015004) and Ministry of Education and Science of the Republic of Kazakhstan (research grant AP08052762).

## Appendix B. Supplementary data

Supplementary data to this article can be found online at <https://doi.org/10.1016/j.petrol.2020.107628>.

## APPENDIX A



$\theta$  – azimuth angle

$a$  – rotation around  $z'$ -axis

$i$  – rotation around  $y$  – axis

**Fig. A1.** Coordinate system for a deviated hole (after Fjaer et al., 2008).

Transformation to a new coordinate system:

$$\begin{aligned} l_{xx'} &= \cos \alpha \cos \beta, l_{xy'} = \sin \alpha \cos \beta, l_{xz'} = -\sin \beta \\ l_{yx'} &= -\sin \alpha, l_{yy'} = \cos \alpha, l_{yz'} = 0 \\ l_{zx'} &= \cos \alpha \sin \beta, l_{zy'} = \sin \alpha \sin \beta, l_{zz'} = \cos \beta \end{aligned}$$

Stresses expressed in (x,y,z) coordinate system:

$$\begin{aligned} \sigma_x^o &= l_{xx'}^2 \sigma_H + l_{xy'}^2 \sigma_h + l_{xz'}^2 \sigma_v \\ \sigma_y^o &= l_{yx'}^2 \sigma_H + l_{yy'}^2 \sigma_h + l_{yz'}^2 \sigma_v \\ \sigma_z^o &= l_{zx'}^2 \sigma_H + l_{zy'}^2 \sigma_h + l_{zz'}^2 \sigma_v \\ \tau_{xy}^o &= l_{xx'} l_{yx'} \sigma_H + l_{xy'} l_{yy'} \sigma_h l_{xz'} + l_{xz'} l_{yz'} \sigma_v \end{aligned}$$

Stresses in elastic zone can be written as follows:

$$\begin{aligned} \sigma_r &= \frac{\sigma_x^o + \sigma_y^o}{2} \left( 1 - \frac{R_i^2}{r^2} \right) + \frac{\sigma_x^o - \sigma_y^o}{2} \left( 1 + 3 \frac{R_i^4}{r^4} - 4 \frac{R_i^2}{r^2} \right) - \cos 2\theta + \tau_{xy}^o \left( 1 + 3 \frac{R_i^4}{r^4} - 4 \frac{R_i^2}{r^2} \right) \cdot \sin 2\theta + p_i \frac{R_i^2}{r^2} \\ \sigma_\theta &= \frac{\sigma_x^o + \sigma_y^o}{2} \left( 1 + \frac{R_i^2}{r^2} \right) - \frac{\sigma_x^o - \sigma_y^o}{2} \left( 1 + 3 \frac{R_i^4}{r^4} \right) - \cos 2\theta \\ -\tau_{xy}^o &\left( 1 + 3 \frac{R_i^4}{r^4} \right) \sin 2\theta - p_i \frac{R_i^2}{r^2} \\ \sigma_z &= \sigma_z^o - \nu_{fr} \left[ 2 \left( \sigma_x^o - \sigma_y^o \right) \frac{R_i^2}{r^2} \cos 2\theta + 4 \tau_{xy}^o \frac{R_i^2}{r^2} \sin 2\theta \right] \end{aligned} \quad (A3)$$

## References

- Al-Awad, M.N.J., 2001. The mechanism of sand production caused by pore pressure fluctuations. *Oil Gas Sci. Technol.* 56, 339–345. <https://doi.org/10.2516/Ogst:2001029>.
- Araujo, E.F., Alzate, G.A., Arbelaez, A., Peña, S., Cardona, A., Naranjo, A., 2014. Analytical prediction model of sand production integrating geomechanics for open hole and cased – perforated wells. *Soc. Pet. Eng.* 171107 <https://doi.org/10.2118/171107-MS>.
- Bratli, R.K., Horsrud, P., Risnes, R., 1983. Rock mechanics applied to the region near a wellbore. 5th ISRM Congress, Melbourne, Australia, pp. 1–17.
- Colmenares, L., Zoback, M.D., 2002. A statistical evaluation of intact rock failure criteria constrained by polyaxial test data for five different rocks. *Int. J. Rock Mech. Min. Sci.* 39, 695–729.
- Consoli, N.C., 2014. A method proposed for the assessment of failure envelopes of cemented sandy soils. *Eng. Geol.* 169, 61–68. <https://doi.org/10.1016/j.enggeo.2013.11.016>.
- Fjaer, E., Holt, R.M., Horsrud, P., Raaen, A.M., Risnes, R., 2008. Petroleum Related Rock Mechanics. In: *Developments in Petroleum Science*, second ed. Elsevier B.V.
- Geilikman, M.B., Dusseault, M.B., Dullien, F.A., 1994. Sand production as a viscoplastic granular flow. International Symposium on Formation Damage Control. Lafayette, Louisiana, pp. 41–50. <https://doi.org/10.2118/27343-ms>.
- Gholami, R., Aadnoy, B., Rasouli, V., Fakhari, N., 2016. An analytical model to predict the volume of sand during drilling and production. *J. Rock Mech. Geotech. Eng.* 8, 521–532. <https://doi.org/10.1016/j.jrmge.2016.01.002>.
- Hayavi, M.T., Abdideh, M., 2017. Establishment of tensile failure induced sanding onset prediction model for cased-perforated gas wells. *J. Rock Mech. Geotech. Eng.* 9, 260–266. <https://doi.org/10.1016/j.jrmge.2016.07.009>.
- Iskaziyev, K., Karabalin, U., Azhgaliyev, D., 2013. Complex study of sedimentary basins is the basis for effective forecast of the oil and gas content in new territories. *Pet. Anal. J.*
- Kozhagulova, A., Hop, N., Zhao, Y., Cheong, S., 2020a. A study on bond breakage behavior of weak Cretaceous Kazakhstani reservoir sandstone analogue. *Geomech. Energy Environ.* 21 <https://doi.org/10.1016/j.gete.2019.100159>.
- Kozhagulova, A., Shabdirova, A., Minh, N.H., Zhao, Y., 2020b. An integrated laboratory experiment of realistic diagenesis, perforation and sand production using large artificial sandstone specimen. *Rock Mech. Geotech. Eng. Under Rev.*
- Kozhagulova, A.A., Shabdirova, A.D., T, G., Minh, N.H., 2018. Bond characteristics of artificial sandstones with sodium silicate cement. 52nd US Rock Mechanics/Geomechanics Symposium. Seattle, Washington.
- Morita, N., Waseda, U., Fuh, G.-F., Burton, B., 2006. Field and laboratory observations of post-failure stabilizations during sand production. SPE Annual Technical Conference and Exhibition, pp. 1–8. Texas, USA.
- Morita, N., Whitfill, D.L., Fedde, O.P., Levik, T.H., 1989. Parametric study of sand production prediction analytical approach. *SPE Prod. Eng.*
- Murzagaliyev, R., 2009. Geology and Development of Karazhanbas High Viscous Oil Field and Modern Production Geotechnologies. Gubkin Russian State University of Oil and Gas.
- Palmer, I., Vaziri, H., Willson, S., Moschovidis, Z., Cameron, J., Ispas, I., 2003. Predicting and managing sand production: a new strategy. Proc. - SPE Annu. Tech. Conf. Exhib. 3949–3961. <https://doi.org/10.2118/84499-MS>.
- Papamichos, E., Cerasi, P., Stenebraten, J., 2010. Sand production rate under multiphase flow and water breakthrough. *Pap. ARMA* 10–340.
- Papamichos, E., Malmanger, E.M., 2001. A sand-erosion model for volumetric sand predictions in a north Sea reservoir. *Engineering* 21–23. <https://doi.org/10.2118/54007-ms>.
- Papamichos, E., Skjaerstein, A., Tronvoll, J., 2000. A volumetric sand production experiment. *Pacific Rocks 2000 Rock Around Rim* 303–310.
- Papamichos, E., Stavropoulou, M., 1998. An erosion-mechanical model for sand production rate prediction. *Int. J. Rock Mech. Min. Sci.* 35, 531–532. [https://doi.org/10.1016/S0148-9062\(98\)00106-5](https://doi.org/10.1016/S0148-9062(98)00106-5).
- Papamichos, E., Vardoulakis, I., Tronvoll, J., Skjærstein, A., 2001. Volumetric sand production model and experiment. *Int. J. Numer. Anal. Methods GeoMech.* 25, 789–808. <https://doi.org/10.1002/nag.154>.
- Rahimi, R., Nygaard, R., 2015. Comparison of rock failure criteria in predicting borehole shear failure. *Int. J. Rock Mech. Min. Sci.* 79, 29–40. <https://doi.org/10.1016/j.ijrmms.2015.08.006>.
- Rios, S., Viana da Fonseca, A., Baudet, B.A., 2014. On the shearing behaviour of an artificially cemented soil. *Acta Geotech.* 9, 215–226. <https://doi.org/10.1007/s11440-013-0242-7>.
- Risnes, R., Bratli, R.K., Horsrud, P., 1982. Sand stresses around a wellbore. *Soc. Petrol. Eng. J.* 22, 883–898. <https://doi.org/10.2118/9650-pa>.
- Shabdirova, A., Minh, N.H., Zhao, Y., Fok, S.C., 2020. The role of plastic zone permeability in sand production in weak sandstone reservoirs. *Under Rev.*
- Skjaerstein, A., Stavropoulou, M., Vardoulakis, I., Tronvoll, J., 1997. Hydrodynamic Erosion: A Potential Mechanism of Sand Production in Weak Sandstones, vol. 34, pp. 3–4.
- Stavropoulou, M., Papanastasiou, P., Vardoulakis, I., 1998. Coupled wellbore erosion and stability analysis. *Int. J. Numer. Anal. Methods GeoMech.* 22, 749–769. [https://doi.org/10.1002/\(SICI\)1096-9853\(199809\)22:9<749::AID-NAG944>3.0.CO;2-K](https://doi.org/10.1002/(SICI)1096-9853(199809)22:9<749::AID-NAG944>3.0.CO;2-K).
- van den Hoek, P.J., Geilikman, M.B., 2005. Prediction of sand production rate in oil and gas reservoirs: field validation and practical use. *SPE Annu. Tech. Conf. Exhib.* <https://doi.org/10.2118/95715-MS>.
- van den Hoek, P.J., Geilikman, M.B., 2003. Prediction of sand production rate in oil and gas reservoirs. *SPE Annu. Tech. Conf. Exhib.* <https://doi.org/10.2118/84496-MIS>.
- Vardoulakis, I., Stavropoulou, M., Papanastasiou, P., 1996. Hydromechanical aspects of sand production problem. *Transport Porous Media* 22, 225–244.
- Willson, S.M., Moschovidis, Z.A., Cameron, J.R., Palmer, I.D., 2002. New model for predicting the rate of sand production. *SPE/ISRM Rock Mech. Conf.* 152–160. <https://doi.org/10.2118/78168-ms>.
- Wu, B., Choi, S.K., Denke, R., Barton, T., Viswanathan, C., Lim, S., Zamberi, M., Shaffee, S., 2016. A new and practical model for amount and rate of sand production. *Offshore Technol. Conf.* 18.
- Yi, X., 2003. Numerical and Analytical Modeling of Sanding Onset Prediction Numerical and Analytical Modeling of Sanding Onset Prediction.
- Younessi, A., Rasouli, V., Wu, B., 2013. Sand production simulation under true-triaxial stress conditions. *Int. J. Rock Mech. Min. Sci.* 61, 130–140. <https://doi.org/10.1016/j.ijrmms.2013.03.001>.
- Zhang, R., Shi, X., Zhu, R., Zhang, C., Fang, M., Bo, K., Feng, J., 2016. Critical drawdown pressure of sanding onset for offshore depleted and water cut gas reservoirs: modeling and application. *J. Nat. Gas Sci. Eng.* 34, 159–169. <https://doi.org/10.1016/j.jngse.2016.06.057>.